Resource usage and gene circuit performance characterization in a cell-free 'breadboard'

Dan Siegal-Gaskins[1,*], Zoltan A. Tuza[2,*], Jongmin Kim[1,*],
Vincent Noireaux[3], and Richard M. Murray[1,4]

1. Division of Biology and Biological Engineering, California Institute of Technology, Pasadena, CA, USA
2. Faculty of Information Technology, Pazmany Peter Catholic University, Budapest, Hungary
3. School of Physics and Astronomy, University of Minnesota, Minneapolis, MN, USA
4. Department of Control and Dynamical Systems, California Institute of Technology, Pasadena, CA, USA

∗ These authors contributed equally to this work.

Abstract

The many successes of synthetic biology have come in a manner largely different from those in other engineering disciplines; in particular, without well-characterized and simplified prototyping environments to play a role analogous to wind-tunnels in aerodynamics and breadboards in electrical engineering. However, as the complexity of synthetic circuits increases, the benefits—in cost savings and design cycle time—of a more traditional engineering approach can be significant. We have recently developed an *in vitro* 'breadboard' prototyping platform based on *E. coli* cell extract that allows biocircuits to operate in an environment considerably simpler than but functionally similar to *in vivo*. The simplicity of the cell-free transcription-translation breadboard makes it a promising tool for rapid biocircuit design and testing, as well as for probing the fundamentals of gene circuit functions that are normally masked by cellular complexity. In this work we characterize the cell-free breadboard using real-time and simultaneous measurements of transcriptional and translational activities of a small set of reporter genes and a transcriptional activation cascade. We determine the effects of promoter strength, gene, and nucleoside triphosphate concentrations on biocircuit properties, and we isolate contributions of the essential components—core RNA polymerase, housekeeping sigma factor, and ribosomes—to overall performance. Importantly, we show how limits on essential resources, particularly those involved in translation steps, are manifested as reduced expression in the presence of orthogonal genes functioning as load processes.

Keywords

synthetic biology, cell-free systems, biological circuit prototyping

Abbreviations

TX: transcription; TL: translation; FP: fluorescent protein; MGapt: malachite green RNA aptamer; UTR: untranslated region; RNAP: RNA polymerase; NTP: nucleoside triphosphate; RBS: ribosome binding site

Introduction

The field of synthetic biology has matured to the point where biological parts are regularly assembled into modestly complex circuits with wide-ranging applications [1]. Unfortunately, the development of new biological circuits typically involves long and costly *ad hoc* design cycles characterized by trial-and-error and lacking the prototyping stage essential to other engineering disciplines. More often than not, designed circuits fail to operate as expected. The reason for these failures is in many cases related to *context*: the poorly characterized environment in which the system is operating [2–4]. This includes the finite and variable (from cell to cell, condition to condition, and time to time) pools of biomolecular resources such as transcription/translation machinery and nucleoside triphosphates (NTPs), weak control over the component DNA concentrations, unpredicted interactions between components and circuits and their cellular hosts (see, e.g., [5,6]), and any number of other system properties with unknown or unknowable effects.

We have recently developed an *in vitro* biomolecular 'breadboard' based on *E. coli* cell extract that provides a functional environment similar to *in vivo* but with significantly reduced complexity [7,8]. DNA and mRNA endogenous to the cells is eliminated during extract preparation, so that transcription-translation circuits of interest may be operated in isolation without interference by a cellular host. The cell-free breadboard also allows for a degree of control over reaction conditions and component concentrations that cannot be achieved *in vivo*. As a prototyping platform, the cell-free breadboard provides for a considerable reduction in circuit design cycle time, not only because of its relative simplicity when compared with *in vivo*, but also because it eliminates much of the lengthy cloning and cell transformation steps typically required in biocircuit development (see, e.g., [9]). Indeed, cell-free applications for synthetic biology are quickly expanding [10, 11]. But beyond its potential as an improved circuit development platform, our cell-free breadboard has another significant advantage: its simplicity reveals important details of biocircuit operation normally masked by cellular complexity.

In this work we show a detailed and quantitative characterization of the cell-free breadboard—an essential precursor to any biocircuit development and testing application—and explore a number of fundamental aspects of biocircuit operation not easily studied *in vivo*. Central to our work is the use of a novel reporter that combines the malachite green RNA aptamer and a fluorescent protein for a real-time and simultaneous read-out of the system's transcription and translation activity. We establish the functional implications of intrinsic biocircuit properties such as component concentration and promoter strength, as well as those of the extrinsic biomolecular resource pool that includes nucleoside triphosphates (NTPs), sigma factors, and other transcription/translation machinery. Importantly, we show how limits on essential resources, particularly those involved at the translational level, manifest themselves in the form of reduced expression and 'crosstalk' between orthogonal genes. Implications for biocircuit prototyping are discussed.

Results

To best characterize transcription- and translation-level performance in the cell-free breadboard platform, we use a reporter construct encoding an optimized green or cyan fluorescent protein (deGFP/deCFP) along with the malachite green RNA aptamer (MGapt) in the 3′ UTR (Figure 1A). The 35-base MGapt sequence contains a binding pocket for the malachite green dye [12] and allows for real-time fluorescence monitoring of RNA dynamics with a temporal resolution significantly higher than what has been previously achieved in cell extract using radio-labeling and gel analysis (e.g., in [13]). The use of MGapt as a measure of RNA was validated using real-time PCR and by comparing deGFP levels with and without the aptamer in the 3′ UTR (Figures S1 and S2).

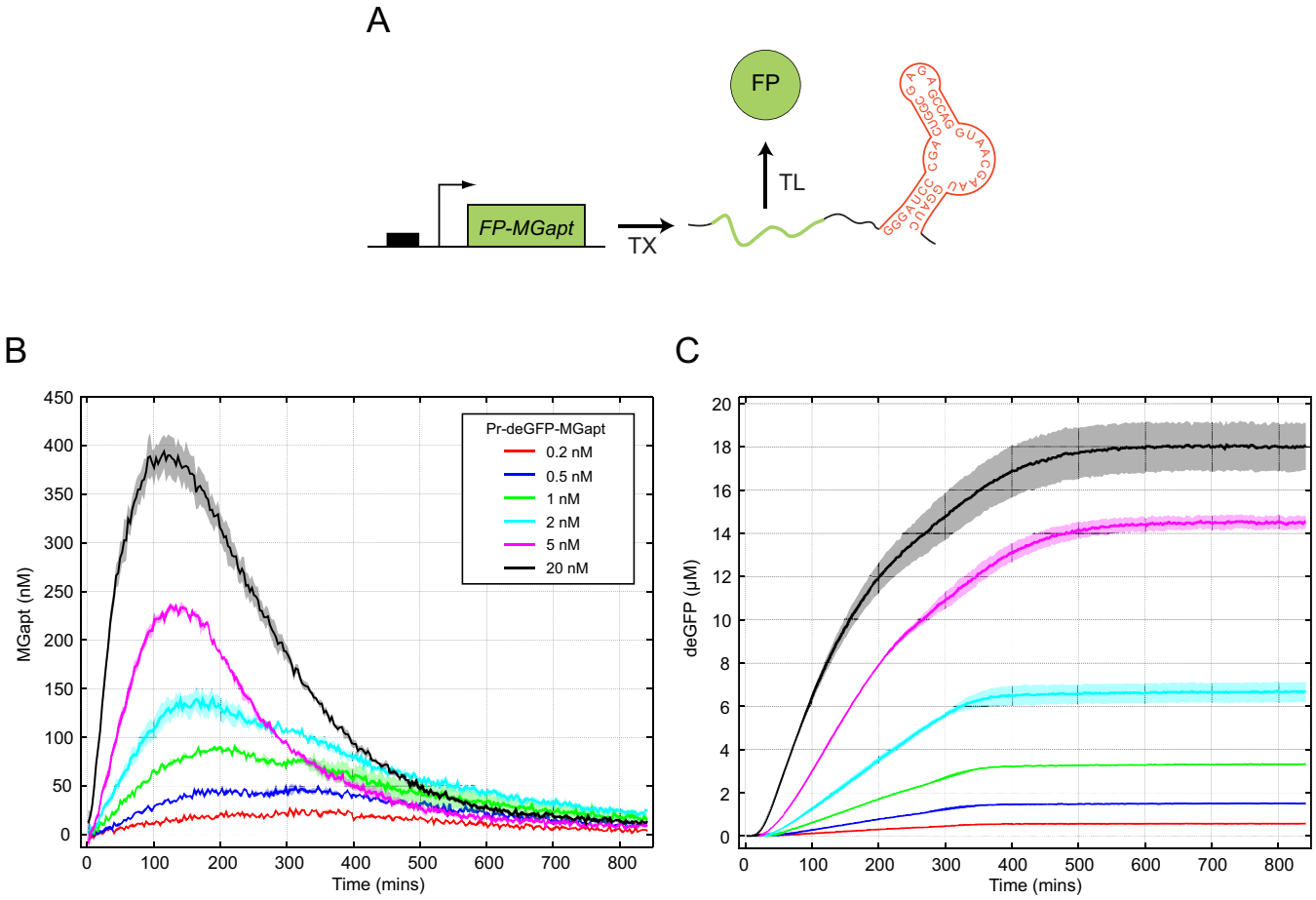

Figure 1: A combined transcription-translation reporter reveals basic features of our cell-free breadboard system. (A) The reporter construct encodes an optimized fluorescent protein (FP) along with the malachite green RNA aptamer (MGapt) in the 3′ UTR. (B) Transcription kinetics reported by MGapt for six different template concentrations. There is a qualitative change in the MGapt profiles between 2 and 5 nM DNA, from curves characterized by relatively broad peaks and slow decays to ones that are more sharply-peaked. (C) Translation kinetics reported by deGFP for six different template concentrations. As protein degradation machinery is absent from the standard platform, protein levels never decrease and the endpoint values represent the total amount of active FP produced. Above 2–5 nM DNA, deGFP expression profiles vary smoothly before saturating, whereas below the profiles can be described as piecewise linear functions with roughly constant positive slope for times $t < t_{end,TL} \sim 330$ minutes and zero slope for $t > t_{end,TL}$. $t_{end,TL}$ appears fixed for all concentrations in this regime.

Constitutive gene expression under standard conditions

The deGFP-MGapt reporter placed under the control of a strong constitutive promoter, Pr (the lambda repressor Cro promoter), and strong untranslated region (UTR) serves as our baseline construct. MGapt expression curves demonstrate complex RNA dynamics that include production via transcription machinery and degradation by RNases (Figure 1B). Saturation of the DNA by the transcription machinery can be seen in the slopes of the MGapt curves during the early stages of the experiment; these early production rates are well described by a Michaelis-Menten–type function with Michaelis constant of ∼24 nM (Figure S3). The absence of a steady-state level of MGapt indicates that RNA production does not continue indefinitely. We note a distinct qualitative change in the MGapt profiles between template DNA concentrations of 2

and 5 nM, from curves characterized by relatively broad peaks and slow decays to ones that are more sharply-peaked.

Protein expression curves (Figure 1C) show simpler translation dynamics—protein degradation machinery is absent from the standard cell-free breadboard—but again we see qualitative differences above and below a 2–5 nM DNA threshold. Above, deGFP production slows continuously before stopping at ~ 500 minutes. Below the threshold the profiles may be described as piecewise linear functions with roughly constant positive slope for times $t < t_{end,TL} \sim 330$ minutes and zero slope for $t > t_{end,TL}$. Given that $t_{end,TL}$ appears fixed for all concentrations in this regime, it is unlikely that the cessation of protein production is due to complete consumption of necessary resources by the translation machinery. Similar results have been noted previously [14] with the suggestion that a number of other processes, including NTP hydrolysis and enzyme denaturation, may lead to early termination of protein synthesis reactions [15, 16].

We use two simple measures to better compare transcription- and translation-level performance under different conditions: MGapt integrated over the course of the experiment ($\int_{t=0}^{t_{end}} \mathrm{MGapt}(t')\mathrm{d}t' = \int \mathrm{MGapt}$) and the concentration of deGFP at the end of the experiment ($\mathrm{deGFP}(t_{end}) = [\mathrm{deGFP}]_{end}$). The choice of these performance metrics is motivated by the relationship between integrated MGapt and deGFP concentrations under 'ideal' conditions: in the absence of protein degradation, and under the naive assumptions of unlimited resources and conditions unchanging with time, a simple model for deGFP production may be written as

$$\frac{\mathrm{d}}{\mathrm{d}t}\mathrm{deGFP}(t) = k_{TL}\,\mathrm{MGapt}(t - t_{mat}) \tag{1}$$

for constants k_{TL} and t_{mat}, and thus deGFP at any time t^* may be expected to be proportional to $\int^{t*}\mathrm{MGapt}$ (with a short delay for deGFP maturation). This model was previously validated for up to one hour of expression [13]. Below the 2–5 nM DNA threshold described above and for times $t < t_{end,TL}$ we find that this proportionality continues to hold true (Figure 2A), although the relationship between $\mathrm{deGFP}(t^*)$ and $\int^{t*}\mathrm{MGapt}$ becomes much less straightforward as resources are consumed and system conditions change with time (see Supporting Information). Plotting $\int\mathrm{MGapt}$ and $[\mathrm{deGFP}]_{end}$ as a function of plasmid concentration (Figure 2B), we see a 'linear' regime in which $[\mathrm{deGFP}]_{end}$ is proportional to DNA concentration and a 'saturation' regime in which $[\mathrm{deGFP}]_{end}$ versus DNA concentration is sublinear. These regimes correspond to the qualitative differences in the MGapt and deGFP expression curves described above. Surprisingly, we see no significant change in $\int\mathrm{MGapt}$ at the transition between regimes.

Transcription, translation, and promoter strength

To determine how promoter strength affects transcription and translation in our cell-free breadboard, we tested the reporter construct under the control of two additional constitutive promoters Pr1 and Pr2 made weaker than Pr by single base mutations in the -35 and -10 region, respectively (see Materials and Methods). We find that the concentration at which the system transitions from the linear regime to the saturation regime is increased for these weaker promoters, up to $\sim$10 nM for Pr1 and $\sim$20 nM for Pr2 (Figure S5). Thus, we see something of a performance trade-off between DNA concentration and promoter strength: a weaker promoter allows for 'linear' performance with higher template concentrations.

The overall performance under different promoters can be summarized and compared in a plot of $[\mathrm{deGFP}]_{end}$ versus $\int\mathrm{MGapt}$, effectively a measure of protein produced per transcript (Figure 3). Worth noting is the dramatic increase in the Pr curve at the regime transition point, an increase not seen for the weaker promoters. This may be explained by the differential transcriptional dynamics in the 'linear' and 'saturation' regimes—distributed versus peaked—coupled with decreasing activity of the translation machinery. Such a time-dependent reduction in translational efficiency, reported in other cell-free systems [14], would mean that although transcription may take place later in the experiment, the resulting transcripts are less translatable.

What is clear from Figure 3 is that the relationship between DNA template concentration, promoter strength, integrated RNA, and final protein concentration is not a simple one; for example, with 2 nM

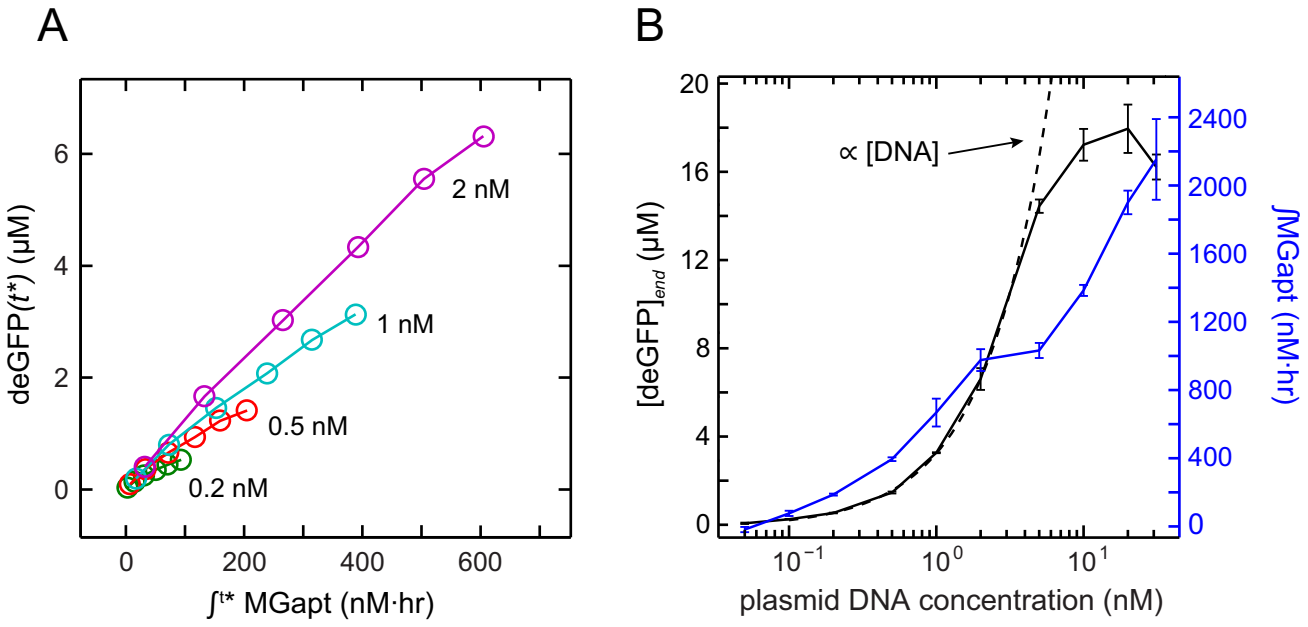

Figure 2: (A) deGFP versus integrated MGapt for the first six hours of expression for a range of DNA template concentrations. The relationship between them is linear as predicted by a simple model (Eq. 1). (B) Endpoint deGFP and integrated MGapt as a function of DNA template concentration. The endpoint deGFP level is proportional to the amount of template up to ∼2–5 nM.

DNA, $\int$MGapt produced using Pr1 and Pr2 is 40% and 15% of the Pr value, respectively, and $[\text{deGFP}]_{end}$ is 11% and 0.4% of that produced by Pr. With 20 nM DNA, the percentages are different: $\int$MGapt produced using Pr1 and Pr2 is 70% and 32% of Pr, respectively, and $[\text{deGFP}]_{end}$ is 30% and 2% of Pr. We note that at this higher concentration, the strong promoter is operating in the 'saturation' regime, while the weaker promoters are not.

The role of NTPs

The standard platform contains the natural NTPs essential for biocircuit operation, in concentrations of 1.5 mM ATP and GTP and 0.9 mM CTP and UTP [17]. Among their many cellular functions, ATP and GTP play a crucial role in translation, and all four NTPs are used in transcription as substrates in the synthesis of RNA. NTPs thus serve to couple a biocircuit's transcription and translation layers together, with an impact that is not intuitively obvious but that can be significant (see, e.g., [18]). As a result, understanding precisely how changes in NTP concentration affect performance is of paramount importance.

We supplemented the system with an additional 1.25 mM of each NTP, an increase of ∼83% ATP/GTP and ∼138% CTP/UTP. In the linear regime, the extra NTPs have little effect on the shapes of the MGapt and deGFP profiles, save for an increase in $t_{end,TL}$ to ∼450–500 minutes (Figure S6). In the saturation regime however, the MGapt curves are broadened dramatically while the deGFP curves are more compressed at late times. The overall effect may be more easily seen on a plot of $[\text{deGFP}]_{end}$ versus $\int$MGapt (Figure 3). We find that the additional NTPs support a ∼30% increase in $[\text{deGFP}]_{end}$ in the linear regime, a result that we primarily attribute to the increase in $t_{end,TL}$. That is, the rate of production is relatively fixed but the productive period is extended. $\int$MGapt also increases at low DNA concentrations. A more surprising result is seen at high DNA concentration, where $\int$MGapt increases considerably but $[\text{deGFP}]_{end}$ is actually reduced by up to 20%. This suggests that NTPs do in fact help at the transcription level but that those excess transcripts are not translatable, and that perhaps the resources used to produce

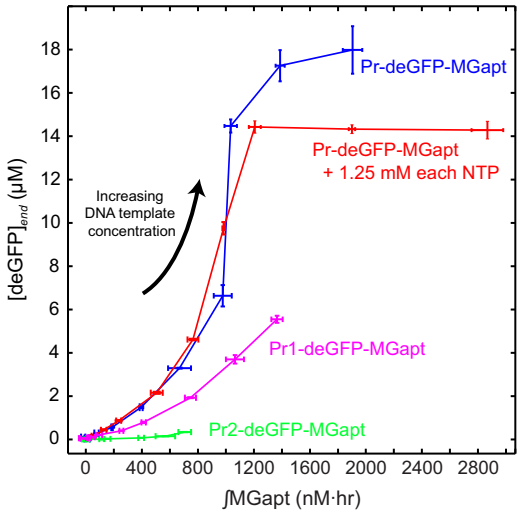

Figure 3: Endpoint deGFP vs integrated MGapt for three different promoters (Pr, Pr1, and Pr2) and with the cell-free breadboard supplemented with 1.25 mM of each of the four NTPs. DNA template concentrations are 0.02–20 nM.

those transcripts may have been taken at the expense of reporter protein production.

Additional 'housekeeping' sigma factors

The association of a sigma factor (σ) with the catalytic core RNA polymerase (RNAP) is necessary for promoter recognition and transcription initiation in bacteria [19]. Thus, both σ and core RNAP are potential bottlenecks on transcription. In the cell-free breadboard, only the *E. coli* 'housekeeping' σ^{70} is present at appreciable concentrations [8]. To address the possibility that σ^{70} is in short supply and that it introduces an additional, NTP-independent limit on transcription capacity as a result, we supplemented the system with a plasmid carrying the σ^{70} gene under the control of the Pr promoter and assessed the system performance. Looking at MGapt kinetics at early times (Figure 4), when resources that might otherwise be consumed in the production of σ^{70} are still plentiful, we see that 0.1–0.5 nM Pr-σ^{70} increases the level of MGapt for all reporter DNA concentrations tested relative to standard conditions. 1 nM Pr-σ^{70} only has a positive effect with 10 nM reporter. Taken together these results suggest that additional σ^{70} does in fact help initiate more transcription events, although the effect is a mild one. We note that the Pr-σ^{70} kinetic traces deviate from the nominal curves at ∼30-40 minutes, a time that allows for the accumulation of the additional σ^{70}. (Further discussion of the effect of additional Pr-σ^{70} can be found in the Supporting Information.)

Performance of a simple transcription-translation cascade

We also investigated the effect of adding an intermediate layer of transcription and translation on our reporters. The 'cascade' consists of constitutively-expressed T7 RNAP under the control of Pr, Pr1, or Pr2 and the deGFP-MGapt construct downstream of a T7-specific promoter (Figure 5). T7 RNAP is convenient to use for this purpose since, unlike the native *E. coli* RNAP, it is a single-subunit RNAP that is easy to incorporate onto a single plasmid, and it does not compete with the core RNAP for sigma factors. This cascade circuit allows us to further determine if NTP consumption by transcription/

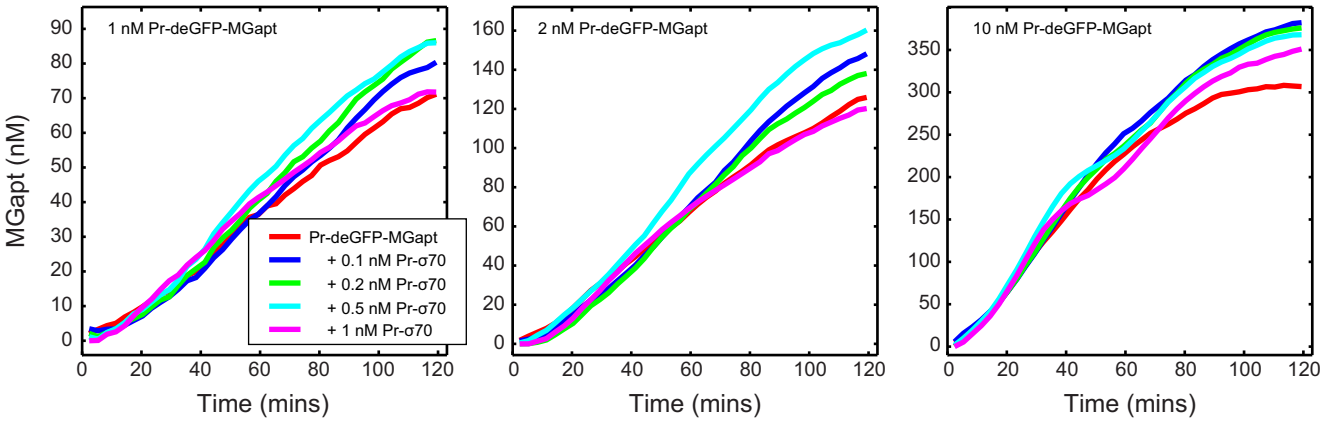

Figure 4: MGapt kinetics in the first 120 min of the experiment with different Pr-σ^{70} and reporter DNA concentrations. Expression under standard conditions is shown in red. The addition of 0.1–0.5 nM Pr-σ^{70} increases MGapt above the nominal case during this time. 1 nM Pr-σ^{70} only has a positive effect with 10 nM reporter.

translation processes is a limiting factor, since the additional layer of transcription and translation would lead to a reduction in output relative to constitutive expression as it consumes more of these resources more quickly. Alternatively, if expression was limited (at least in part) by a reduction in the activity of the native RNAP, the introduction of T7 RNAP may extend the lifetime of the system.

There are substantial qualitative differences in T7 cascade expression as compared with a single-stage constitutive promoter. RNA increases rapidly and exhibits a long, slow decay (see, e.g., Figure S7), and there is a ∼30-60 minute delay in protein expression (see, e.g., Figure S8). A higher reporter DNA concentration leads to a shorter delay and faster rise in expression, but the final deGFP concentration is often below the level achieved with a lower reporter concentration. This suggests a trade-off in cascade-driven protein production that may be the result of fuel consumption: if deGFP is produced more quickly, then the production appears to arrest sooner.

We find that the T7 cascade protein output is dictated by the concentration of the first-stage T7 RNAP plasmid and the identity of the promoter that drives T7 RNAP expression (Figure 5). Weaker promoters (Pr1 and Pr2) controlling T7 RNAP expression lead to a wide range of deGFP levels with only small variations in the T7 RNAP concentration, and for any fixed concentration of the T7 RNAP plasmid, adjusting the reporter concentration over an order of magnitude does not affect deGFP output appreciably. When the strong Pr promoter is used, deGFP levels saturate at a level independent of the Pr-T7 RNAP concentration while MGapt levels vary substantially. The T7 cascade thus provides for independent tuning of RNA and protein outputs. Interestingly, we find regions of overlap where cascades with high concentrations of weaker first-stage promoters behave identically to low concentrations of stronger first-stage promoters. This equivalence was not present with the one-stage simple expression and may be due to the fact that in all versions of the cascade the promoters driving deGFP are identical.

In the simple expression case we found that adding NTPs to the system led to a considerable increase in transcription in the 'saturation' regime, but that the excess transcripts were not translated, and moreover that the resources used to produce those transcripts may have been taken at the expense of reporter protein production. We thus set out to see how the same addition of NTPs affects output of the T7 cascade with a strong first-stage promoter. As before, we supplemented the system with an additional 1.25 mM of each NTP. The resulting kinetics can be seen in Figures S9 and S10, and compared with Figures S7 and S8. Again we see a significant increase in the transcriptional activity; peaks are taller and broadened and the differences between different PT7-deGFP-MGapt concentrations are more pronounced. And while we do

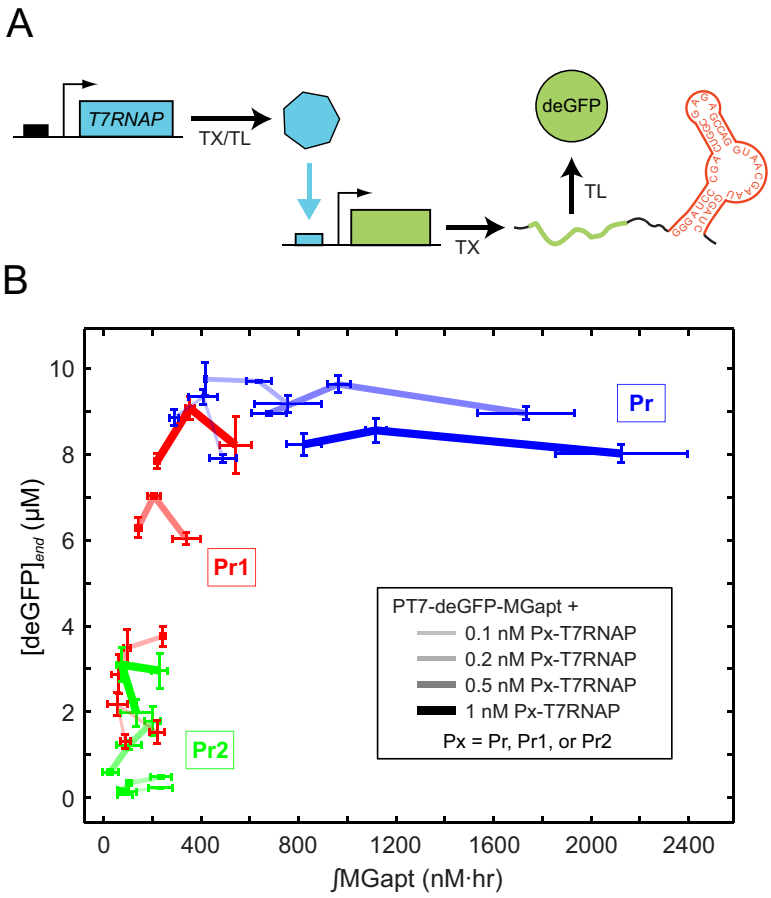

Figure 5: (A) The T7 cascade consists of constitutively-expressed T7 RNAP under the control of Pr, Pr1, or Pr2 and the deGFP-MGapt construct downstream of a T7-specific promoter. (B) Endpoint deGFP versus integrated MGapt for the T7 cascade with Pr-, Pr1-, or Pr2-T7 RNAP (0.1, 0.2, 0.5, and 1 nM) upstream of the PT7-deGFP-MGapt reporter (1, 2, and 10 nM).

not see a decrease in deGFP as we did with the Pr-deGFP-MGapt construct, there is little benefit to excess NTPs at the translational level.

Resource sharing and crosstalk between orthogonal genes

Recent work has highlighted indirect coupling between genes, or 'crosstalk', as a prominent side-effects of resource sharing in biocircuits [20–26]. Resources include those which are consumed during circuit operation (e.g., NTPs) as well as transcription/translation machinery that is present in limited amounts and that different parts of the circuit are forced to share. To clearly distinguish between crosstalk at the transcription stage (that may arise due to competition for RNAP or σ^{70}) and at the translation stage (arising from, e.g., a limited ribosome pool), we assayed system performance with the reporter Pr-deCFP-MGapt and two different orthogonal loads present: (1) deGFP, driven by the same Pr promoter as the reporter, and (2) the same Pr-deGFP construct but with the ribosome binding site (RBS) deleted (Pr-ΔRBS-deGFP). Crosstalk at the transcription and translation levels appears as changes in MGapt and deCFP fluorescence, respectively; with the Pr-ΔRBS-deGFP, any crosstalk must be strictly transcriptional as there is no RBS that can sequester ribosomes away from the deCFP reporter.

We find that an increase in loading generally leads to a decrease in reporter expression, although it affects the transcription and translation levels differently (Figure 6). For example, there is a similar ∼250

nM·hr variation in $\int$MGapt as load increases for all reporter concentrations. At the translation level, however, the effect is highly dependent on load and reporter concentrations: the influence of the load on $[\text{deCFP}]_{end}$ is small at 1 nM reporter DNA but significant at 10 nM reporter. Thus, as the reporter DNA concentration increases, and the resources needed to produce reporter protein are more in demand, the translational crosstalk becomes much more pronounced. This also highlights the maximum translation capacity of the system that limits the total amount of protein that can be produced; as $[\text{deGFP}]_{end}$ goes up, $[\text{deCFP}]_{end}$ necessarily goes down. The top right corner of the $[\text{deGFP}]_{end}$–$[\text{deCFP}]_{end}$ plot in Figure 6 represents a translation performance regime that appears to be inaccessible.

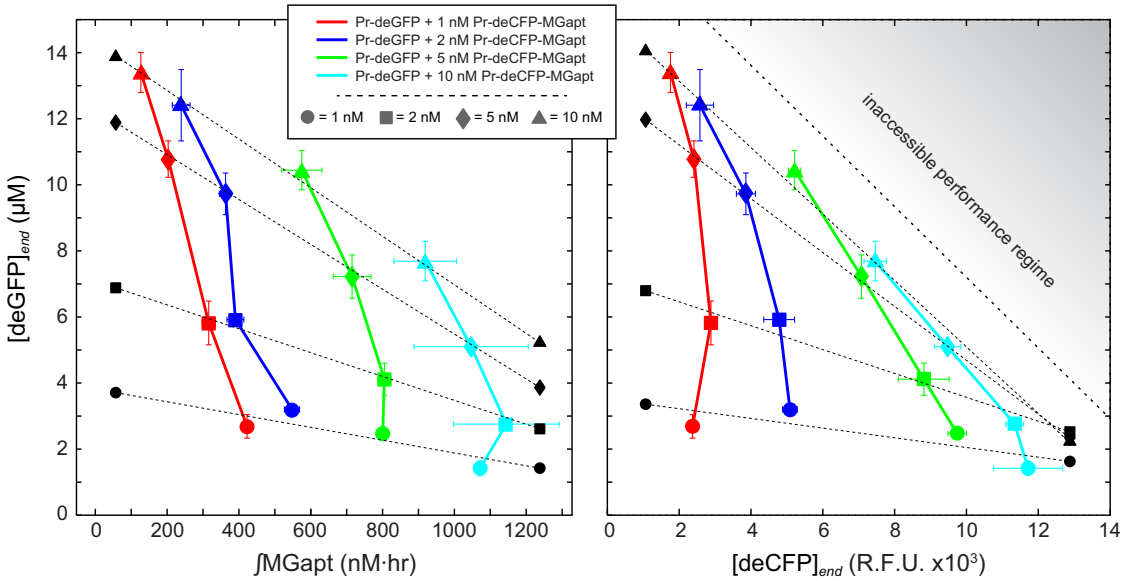

Figure 6: Endpoint deGFP versus integrated MGapt (left) and versus endpoint deCFP (right) following competitive expression of Pr-deCFP-MGapt and Pr-deGFP constructs. The variation in $\int$MGapt with increasing load is similar for all reporter concentrations, whereas at the translation level the crosstalk effect is highly dependent on load and reporter concentrations. There is a maximum translation capacity to the system that limits the total amount of protein that can be produced, as indicated by the inaccessible performance regime. Symbols indicate different concentrations of Pr-deGFP: ● = 1 nM, ■ = 2 nM, ♦ = 5 nM, and ▲ = 10 nM.

The loading effects seen in Figure 6 suggest that translation resources may be more limiting to system performance. To confirm this result, we compare the $\int$MGapt–$[\text{deCFP}]_{end}$ relationships for the Pr-deGFP and Pr-ΔRBS-deGFP constructs (Figure 7). When the RBS is present, in general we see that an increase in load leads to a decrease in $\int$MGapt and $[\text{deCFP}]_{end}$ (Figure 6, left). When the RBS is absent (Figure 6, right), for the most part the load has no effect on performance, except for at high concentrations of both load and reporter, at which point we note a decrease in $[\text{deCFP}]_{end}$ and increase in $\int$MGapt.

Discussion

Interest in simplified *in vitro* environments that approximate *in vivo* conditions is rooted in the desire to build and better understand biological circuits without the confounding factors that exist in live cells. Key to the success of these development and testing platforms is detailed and quantitative characterization. In this work we characterized a recently-developed, cell extract–based 'breadboard' which we then applied to the study of how biomolecular resources are used and shared in simple biocircuits. A novel reporter

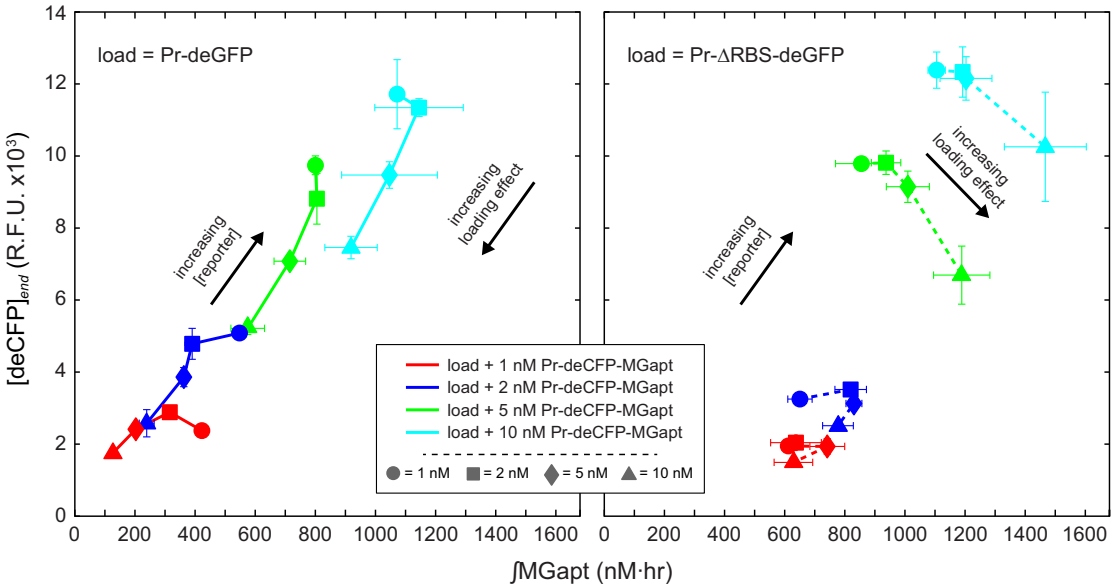

Figure 7: Effect of orthogonal Pr-deGFP (left) and Pr-ΔRBS-deGFP (right) loads on reporter expression. Increasing Pr-deGFP tends to decrease both $\int$MGapt and $[\text{deCFP}]_{end}$. Without the RBS, only when load and reporter concentrations are high do we see a crosstalk effect: a decrease in $[\text{deCFP}]_{end}$ and increase in $\int$MGapt. Load concentrations are indicated as: ● = 1 nM, ■ = 2 nM, ♦ = 5 nM, and ▲ = 10 nM.

construct consisting of the malachite green RNA aptamer and a fluorescent protein allowed us to monitor transcription and translation simultaneously and in real-time. The use of the malachite green RNA aptamer may offer advantage over molecular beacons and binary probes [27, 28] in terms of wider dynamic range and faster response times. An analogous strategy connecting an RNA aptamer that mimics GFP [29] with fluorescent proteins spurred interest in concurrent measurement of transcription-translation activities *in vivo* [30, 31]. Recent studies have indicated that MGapt is also compatible with *in vivo* characterization of synthetic circuits [], rendering this study relevant to *in vivo* studies as well as expanding the toolsets for real-time RNA monitoring with different spectral properties. Our results confirmed that transcriptional activity is a good predictor of translation-level behavior within a linear regime of DNA template concentrations for up to 6 hrs or more, beyond typical results for batch-mode cell-free reactions [14, 32]. On the other hand, the transcriptional and translational capacity of the system shows saturation dependent on different factors, adding to the consensus that there is significant value in the development and use of reliable transcription-translation reporters for concurrent mRNA and protein measurement.

In what follows we further discuss the connections between cell-free and *in vivo* results, and the implications of this work for more effective biocircuit prototyping.

Relevance for *in vivo*

While it can be expected that specific circuit behaviors will manifest themselves to different degrees in cell-free systems versus *in vivo*, cell-free work has significant potential for contributing to our understanding of how circuits function in living systems. One example may be found in our 'resource competition' assays, through which we were able to quickly and clearly observe the translation machinery serving as a significant limiting resource. While a translational bottleneck has been noted in cell-free systems previously [33], a systematic characterization of loads on the system at transcription and translation levels has not been reported. Similar ribosome loading effects have been suggested by recent theoretical work [24] and several other studies on ribosome utilization [25,34–36], despite the fact that live cells are able to produce additional

translation machinery.

Other consequences of a limited ribosome pool may also be found *in vivo*. For example, it has been established that ribosomes protect mRNAs from the action of endonucleases [37] and that ribosome spacing is a determinant of degradation rate [38]. Thus, if demands on a system are such that the available ribosome pool is insufficient to densely cover the number of transcripts, increased endonucleolytic activity would lead to an increase in the RNA degradation rate constant. Interestingly, a sharp increase in degradation rate is precisely what is seen in the MGapt expression profiles when the system transitions from the 'linear' to the 'saturation' regime (Figure 1B).

Of course, ribosomes are not the only molecular resource that can find themselves in short supply, in our cell-free system or *in vivo*. It was recently shown that the *E. coli* ClpXP protein degradation machinery can be overloaded, leading to significant crosstalk between unrelated networks [21]. More recent theoretical work has suggested that competition for a relatively small number of RNases by a large number of RNA molecules can also lead to crosstalk [18]. Evidence for this form of crosstalk may be found in our results: in the increase in $\int$MGapt that occurs when the untranslated ΔRBS-deGFP load is added in amounts higher than or comparable to the reporter (Figure 7). In this case, the load presents a large number of new targets for degradation enzymes, drawing them away from the RNA reporter and thus indirectly leading to the increase in $\int$MGapt. We are currently unaware of *in vivo* results demonstrating crosstalk-via-RNases; however, given the ribosome loading effects seen in both cell-free and *in vivo* systems, it is an intriguing possibility worthy of exploration, especially for RNA-based synthetic regulatory circuits [39–41].

And there are still other examples of how the cell-free breadboard may be used to predict or confirm various effects that arise in cells due to resource limits. In a recent modeling study it was suggested that different combinations of promoter and RBS strengths can result in comparable protein output with different loads on the cellular expression machinery, and that codon usage can introduce a bottleneck that impacts the expression of other genes [42]. The degree of precise control that exists in the cell-free breadboard—for example, control over DNA concentration and known induction levels without an intervening cell membrane—makes it an ideal platform for investigating this and other related questions.

On biocircuit prototyping

Despite recent developments in standardized part libraries and rapid assembly tools (e.g., [43, 44]), synthetic biology still lacks the accepted prototyping platforms and protocols common to other engineering disciplines. For the purposes of prototyping, one particular advantage of our cell-free breadboard is the rapid testing cycle it permits: save for the initial cloning, transformation, and plasmid preparation, none of the individual assays performed in this work required the many hours of cell treatment typically needed for *in vivo* studies. With plasmids in hand, the time from cell-free experiment setup to first results is a matter of minutes.

Problems associated with limits on the cell-free breadboard system capacity may be mitigated when operating in regimes that yield predictable response; the 'linear' regime, for example, where the protein production rate is constant until a well-defined end time and the amount of protein is proportional to template DNA concentration. The 'linear' regime boundaries can change with promoter strength and NTP concentration, as shown in Figure 8. But even when the strongest promoter Pr is used, we find that we can achieve $\sim$6 hours of predictable performance, with measurable FP signal over 3 orders of magnitude of template DNA concentrations. We advocate using the 'linear' regime for cell-free circuit testing or other applications that require linear response. The 'saturation' regime may be used when maximum yield is desired but the linearity of the DNA–protein relationship is not essential.

And there are a number of ways in which limits on the capacity of the cell-free breadboard may be raised. The functional lifetime of the system, which in bulk operation is limited by unidentified mechanisms reducing the activity of the transcription/translation machinery, may be increased using dialysis membranes and vesicles, up to 16 and 100 hours, respectively [8, 45]. Reaction times may be further extended with the

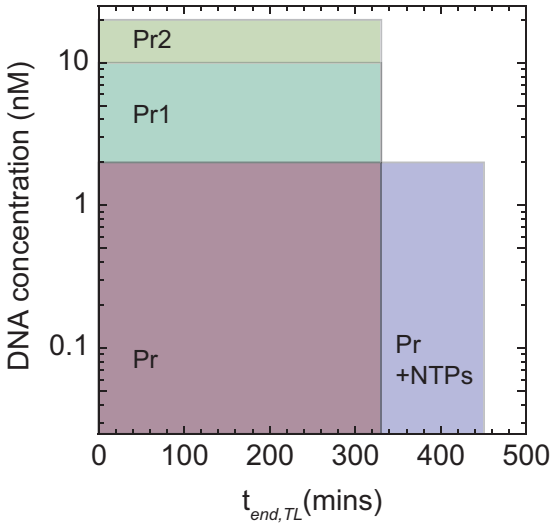

Figure 8: DNA concentration and protein production time boundaries of the 'linear' regime.

use of microfluidics or other continuous-flow devices, as demonstrated with other cell-free environments [32, 46]. Also, the addition of purified proteins such as T7 RNAP or σ^{70} could potentially support an increase in capacity at no additional cost to the system; in related work it has been shown that purified GamS protein can be added to prevent degradation of linear DNA [9]. Ideally, a combination of strategies should be employed to take maximum advantage of the cell-free breadboard. The ease with which these strategies can be employed, along with the relative simplicity of the system and the control that it offers, makes it a promising platform for synthetic biocircuit prototyping.

Materials and Methods

Cell-free system and reactions

The breadboard environment consists of a crude cytoplasmic extract from *E. coli* containing soluble proteins, including the entire endogenous transcription-translation machinery and mRNA and protein degradation enzymes [7,8]. Detailed instructions for extract preparation can be found in [17]. To avoid variation between different extract preparations we used the same batch of extract for all experiments. Reactions took place in 10 μl volumes at 29°C. Measurements were made in a Biotek plate reader at 3 minute intervals using excitation/emission wavelengths set at 610/650 nm (MGapt), 485/525 nm (deGFP), and 433/475 nm (deCFP). No significant toxicity was observed for typical deGFP expression experiments when up to 20 μM malachite green (MG) dye was included in the reaction; the MG dye concentration was thus fixed at 10 μM for all experiments.

Fluorescence measurements and reporters

Real-time fluorescence monitoring of mRNA dynamics was performed using the malachite green aptamer (MGapt) [12] incorporated in the 3′ UTR of the fluorescent protein reporter genes, 15 bases downstream of the stop codons. This location of MGapt insertion was chosen after a number of other possible locations were tested and found to give less accurate measures of RNA dynamics. For example, incorporation of MGapt within the 5′ UTR upstream of the RBS led to decreased RNA stability, a result that may be due

to the preference of 5′ end degradation by the dominant endonuclease in *E. coli*, RNase E [47]. This is consistent with a recent study on the Spinach fluorescent RNA aptamer [30] in which it was reported that incorporation of the aptamer in the 3′ UTR region led to stronger fluorescence than in the 5′ UTR. It was also found that a 6-base spacing between the stop codon of deGFP and MGapt affected the protein expression level to some extent, but a 10-base and 15-base spacing showed equivalent MGapt fluorescence signal levels without affecting protein expression. The fluorescent reporter variants deGFP and deCFP were previously designed to be more translatable in the cell-free system [7]. The UTR controlling translation of deGFP (eGFP-Δ_{6-229}) and deCFP contained the T7 gene *10* leader sequence for highly efficient translation initiation [7]. All the ORFs were terminated by T500 except for the PT7-deGFP-MGapt construct which contained T7 terminator.

Plasmids and Bacterial strains

Plasmids was created using standard cloning methods. The plasmid pBEST-Luc (Promega) was used as a template for all constructs except for the PT7-deGFP-MGapt construct which was derived from the plasmid pIVEX2.3d (Roche). The same antibiotic resistance gene was used with each plasmid to ensure that any burden on the system due to the expression of these 'background' proteins was the same for each construct. All plasmids used are listed in Table S1. Plasmid DNAs used in cell-free experiments were prepared using Qiagen Plasmid Midi prep kits. *E. coli* strains KL740 (which contains lambda repressor to control for Pr promoter) or JM109 were used. LB media with 100 μg/mL carbenicillin was used to culture cells.

Promoters Pr1 and Pr2 were each modified from Pr with a single base mutation in the -35 and -10 region, respectively. The sequences, with mutations highlighted by □, are

Pr: TGAGCTAACACCGTGCGTGTTGACAATTTTACCTCTGGCGGTGATAATGGTTGCA

Pr1: TGAGCTAACACCGTGCGTGT$\boxed{\text{A}}$GACAATTTTACCTCTGGCGGTGATAATGGTTGCA

Pr2: TGAGCTAACACCGTGCGTGTTGACAATTTTACCTCTGGCGGTG$\boxed{\text{C}}$TAATGGTTGCA

Preparation of pure mRNA and qRT-PCR

RNA was transcribed using a linear template PCR-amplified from pIVEX2.3d PT7-deGFP-MGapt including T7 promoter and T7 terminator region. The transcription reaction was prepared as a total volume of 100 μL with 0.1 μM linear DNA template, 20% (v/v) T7 RNA polymerase (Cellscript), 7.5 mM each NTP (Epicentre), 24 mM $MgCl_2$ (Sigma), 10% (v/v) 10× transcription buffer, and 1% (v/v) thermostable inorganic pyrophosphatase (New England Biolabs). After an overnight incubation at 37°C, the reaction mixture was run on 1% agarose gel, RNA bands that correpond to full-length transcript were excised and eluted from gel by the Freeze-N-Squeeze column (Biorad) and resuspended in water. Concentrations of purified RNA were determined spectrophotometrically using Nanodrop.

For qRT-PCR, 1 μL samples were taken at different time points from a tube containing reaction mixture at 29°C and diluted 50-fold in water. These samples were stored at -80°C until used. Afterward the samples were further diluted to a final dilution of 1:5000. Two μL of samples were analyzed in 50 μL reactions of the Power SYBR Green RNA-to-CT 1-Step kit (Life Technologies) in the MX3005 real-time PCR machine (Agilent Technologies). Primers amplified a region of the deGFP gene closer to its 3′ end (424-597 nt) and were used at 0.3 μM concentrations. Concentrations of deGFP-MGapt RNA in the sample were determined from a standard curve of dilutions of purified mRNA in a range from 0.6 to 60 pM mRNA per PCR reaction.

Acknowledgments

The authors would like to thank Eduardo Sontag and members of the Murray Group for helpful discussions. This research is funded in part by the Gordon and Betty Moore Foundation through Grant GBMF2809 to the Caltech Programmable Molecular Technology Initiative, and by the Defense Advanced Research Projects Agency (DARPA/MTO) Living Foundries program, contract number HR0011-12-C-0065. Z.A.T. was partially supported by grants TAMOP-4.2.1-B-11/2/KMR-2011-0002, TAMOP-4.2.2./B-10/1-2010-0014 and OTKA NF 104706.

The views and conclusions contained in this document are those of the authors and should not be interpreted as representing officially policies, either expressly or implied, of the Defense Advanced Research Projects Agency or the U.S. Government.

References

[1] Allen A Cheng and Timothy K Lu. Synthetic biology: an emerging engineering discipline. *Annu Rev Biomed Eng*, 14:155–178, 2012.

[2] Stefano Cardinale and Adam P Arkin. Contextualizing context for synthetic biology - identifying causes of failure of synthetic biological systems. *Biotechnol J*, 7(7):856–866, July 2012.

[3] Caleb J Bashor and James J Collins. Insulating gene circuits from context by RNA processing. *Nat Biotechnol*, 30(11):1061–1062, November 2012.

[4] Stefano Cardinale, Marcin Pawel Joachimiak, and Adam P Arkin. Effects of Genetic Variation on the *E.* coli Host-Circuit Interface. *Cell Reports*, 4(2):231–237, July 2013.

[5] P Marguet, Y Tanouchi, E Spitz, C Smith, and L You. Oscillations by minimal bacterial suicide circuits reveal hidden facets of host-circuit physiology. *PLoS ONE*, 5(7):e11909, 2010.

[6] Cheemeng Tan, Philippe Marguet, and Lingchong You. Emergent bistability by a growth-modulating positive feedback circuit. *Nat Chem Biol*, 5(11):842–848, November 2009.

[7] Jonghyeon Shin and Vincent Noireaux. Efficient cell-free expression with the endogenous E. Coli RNA polymerase and sigma factor 70. *J Biol Eng*, 4(8), 2010.

[8] Jonghyeon Shin and Vincent Noireaux. An E. coli Cell-Free Expression Toolbox: Application to Synthetic Gene Circuits and Artificial Cells. *ACS Synth Biol*, 1(1):29–41, January 2012.

[9] Zachary Z Sun, Enoch Yeung, Clarmyra A Hayes, Vincent Noireaux, and Richard M Murray. Linear DNA for rapid prototyping of synthetic biological circuits in an Escherichia coli based TX-TL cell-free system. *Submitted*, 2013.

[10] C Eric Hodgman and Michael C Jewett. Cell-free synthetic biology: thinking outside the cell. *Metabolic Engineering*, 14(3):261–269, May 2012.

[11] James Chappell, Kirsten Jensen, and Paul S Freemont. Validation of an entirely in vitro approach for rapid prototyping of DNA regulatory elements for synthetic biology. *Nucleic Acids Res*, 41(5):3471–3481, March 2013.

[12] Dilara Grate and Charles Wilson. Laser-mediated, site-specific inactivation of RNA transcripts. *Proc Natl Acad Sci USA*, 96:6131–6136, 1999.

[13] Eyal Karzbrun, Jonghyeon Shin, Roy Bar-Ziv, and Vincent Noireaux. Coarse-grained dynamics of protein synthesis in a cell-free system. *Phys Rev Lett*, 106(4):048104, January 2011.

[14] Tobias Stögbauer, Lukas Windhager, Ralf Zimmer, and Joachim O Rädler. Experiment and mathematical modeling of gene expression dynamics in a cell-free system. *Integr Biol*, 4(5):494–501, May 2012.

[15] Michael C Jewett and James R Swartz. Substrate replenishment extends protein synthesis with an in vitro translation system designed to mimic the cytoplasm. *Biotechnol Bioeng*, 87(4):465–472, August 2004.

[16] D M Kim and J R Swartz. Prolonging cell-free protein synthesis with a novel ATP regeneration system. *Biotechnol Bioeng*, 66(3):180–188, 1999.

[17] Zachary Z Sun, Clarmyra A Hayes, Jonghyeon Shin, Filippo Caschera, Richard M Murray, and Vincent Noireaux. Protocols for Implementing an Escherichia coli Based TX-TL Cell-Free Expression System for Synthetic Biology. *J Vis Exp*, (79), 2013.

[18] Enoch Yeung, Jongmin Kim, Ye Yuan, Jorge Goncalves, and Richard M Murray. Quantifying crosstalk in biochemical systems. In *51st IEEE Conference on Decision and Control (CDC)*, pages 5528–5535, Maui, HI, December 2012.

[19] Sofia Österberg, Teresa del Peso-Santos, and Victoria Shingler. Regulation of alternative sigma factor use. *Annu Rev Microbiol*, 65:37–55, 2011.

[20] Dan Siegal-Gaskins, Vincent Noireaux, and Richard M Murray. Biomolecular resource utilization in elementary cell-free gene circuits. In *American Control Conference (ACC), 2013*, pages 1531–1536, 2013.

[21] Natalie A Cookson, William H Mather, Tal Danino, Octavio Mondragón-Palomino, Ruth J Williams, Lev S Tsimring, and Jeff Hasty. Queueing up for enzymatic processing: correlated signaling through coupled degradation. *Mol Syst Biol*, 7:561, 2011.

[22] Matthew Scott, Carl W Gunderson, Eduard M Mateescu, Zhongge Zhang, and Terence Hwa. Interdependence of cell growth and gene expression: origins and consequences. *Science*, 330(6007):1099–1102, November 2010.

[23] William H Mather, Natalie A Cookson, Jeff Hasty, Lev S tsimring, and Ruth J Williams. Correlation resonance generated by coupled enzymatic processing. *Biophys J*, 99(10):3172–3181, November 2010.

[24] William H Mather, J Hasty, L S Tsimring, and R J Williams. Translational Cross Talk in Gene Networks. *Biophys J*, 2013.

[25] Dominique Chu, David J Barnes, and Tobias von der Haar. The role of tRNA and ribosome competition in coupling the expression of different mRNAs in Saccharomyces cerevisiae. *Nucleic Acids Res*, 39(15):6705–6714, August 2011.

[26] Y Rondelez. Competition for Catalytic Resources Alters Biological Network Dynamics. *Phys Rev Lett*, 108(1):018102, 2012.

[27] Salvatore A.E. Marras, Sanjay Tyagi, and Fred Russell Kramer. Real-time assays with molecular beacons and other fluorescent nucleic acid hybridization probes. *Clinica Chimica Acta*, 363:48–60, 2006.

[28] Henrike Niederholtmeyer, Ling Xu, and Sebastian J. Maerkl. Real-time mRNA measurement during an in vitro transcription and translation reaction using binary probes. *ACS Synth Biol*, 2:411–417, 2013.

[29] Jeremy S. Paige, Karen Wu, and Samie R. Jaffrey. RNA mimics of green fluorescent protein. *Science*, 333:642–646, 2011.

[30] Georgios Pothoulakis, Francesca Ceroni, Benjamin Reeve, and Tom Ellis. The Spinach RNA Aptamer as a Characterization Tool for Synthetic Biology. *ACS Synth Biol*, September 2013.

[31] Pauline van Nies, Zohreh Nourian, Maurits Kok, Roeland van Wijk, Jonne Moeskops, Ilja Westerlaken, Jos M Poolman, Rienk Eelkema, Jan H van Esch, Yutetsu Kuruma, Takuya Ueda, and Christophe Danelon. Unbiased Tracking of the Progression of mRNA and Protein Synthesis in Bulk and in Liposome-Confined Reactions. *Chembiochem*, 14(15):1963–1966, October 2013.

[32] Henrike Niederholtmeyer, Viktoria Stepanova, and Sebastian J Maerkl. Implementation of cell-free biological networks at steady state. *Proc Natl Acad Sci USA*, 110(40):15985–15990, October 2013.

[33] Vincent Noireaux, Roy Bar-Ziv, and Albert Libchaber. Principles of cell-free genetic circuit assembly. *Proc Natl Acad Sci USA*, 100(22):12672–12677, October 2003.

[34] J Vind, M A Sørensen, M D Rasmussen, and S Pedersen. Synthesis of proteins in Escherichia coli is limited by the concentration of free ribosomes. Expression from reporter genes does not always reflect functional mRNA levels. *J Mol Biol*, 231(3):678–688, June 1993.

[35] Namiko Mitarai, Kim Sneppen, and Steen Pedersen. Ribosome collisions and translation efficiency: Optimization by codon usage and mRNA destabilization. *Journal of Molecular Biology*, 382:236–245, 2008.

[36] Michael A. Sørensen and Steen Pedersen. Absolute in vivo translation rates of individual codons in escherichia coli: the two glutamic acid codons GAA and GAG are translated with a threefold difference in rate. *Journal of Molecular Biology*, 222:265–280, 1991.

[37] Atilio Deana and Joel G Belasco. Lost in translation: the influence of ribosomes on bacterial mRNA decay. *Genes Dev*, 19(21):2526–2533, November 2005.

[38] Margit Pedersen, Søren Nissen, Namiko Mitarai, Sine Lo Svenningsen, Kim Sneppen, and Steen Pedersen. The functional half-life of an mRNA depends on the ribosome spacing in an early coding region. *J Mol Biol*, 407(1):35–44, March 2011.

[39] Farren J Isaacs, Daniel J Dwyer, Chunming Ding, Dmitri D Pervouchine, Charles R Cantor, and James J Collins. Engineered riboregulators enable post-transcriptional control of gene expression. *Nat Biotechnol*, 22:841–847, 2004.

[40] Julius B. Lucks, Lei Qi, Vivek K. Mutalik, Denise Wang, and Adam P. Arkin. Versatile RNA-sensing transcriptional regulators for engineering genetic networks. *Proc Natl Acad Sci USA*, 108:8617–8622, 2011.

[41] Guillermo Rodrigo, Thomas E. Landrain, and Alfonso Jaramillo. De novo automated design of small rna circuits for engineering synthetic riboregulation in living cells. *Proc Natl Acad Sci USA*, 109:15271–15276, 2012.

[42] Rhys Algar, Tom Ellis, and Guy-Bart Stan. Modelling the burden caused by gene expression: an in silico investigation into the interactions between synthetic gene circuits and their chassis cell. *arXiv*, September 2013.

[43] Kevin D Litcofsky, Raffi B Afeyan, Russell J Krom, Ahmad S Khalil, and James J Collins. Iterative plug-and-play methodology for constructing and modifying synthetic gene networks. *Nat Meth*, 9(11):1077–1080, November 2012.

[44] Sean C Sleight and Herbert M Sauro. Randomized BioBrick Assembly: A Novel DNA Assembly Method for Randomizing and Optimizing Genetic Circuits and Metabolic Pathways. *ACS Synth Biol*, July 2013.

[45] Vincent Noireaux and Albert Libchaber. A vesicle bioreactor as a step toward an artificial cell assembly. *Proc Natl Acad Sci USA*, 101(51):17669–17674, December 2004.

[46] Qian Mei, Ruba Khnouf, Andrew Simon, and Z Hugh Fan. Protein synthesis in a device with nanoporous membranes and microchannels. *Lab Chip*, 10(19):2541–2545, October 2010.

[47] George A Mackie. RNase E: at the interface of bacterial RNA processing and decay. *Nat Rev Microbiol*, 11(1):45–57, January 2013.

Supporting Information

Relationship between integrated MGapt and deGFP concentration

Throughout this work we have used the amount of MGapt integrated over the course of the experiment ($\int_{t=0}^{t_{end}} \text{MGapt}(t')\text{d}t' = \int \text{MGapt}$) and the concentration of deGFP at the end of the experiment (deGFP(t_{end}) = $[\text{deGFP}]_{end}$) as measures of transcription- and translation-level performance. While the proportionality between deGFP(t^*) and $\int^{t*}$MGapt would hold true for all times t^* in the absence of protein degradation and under the naive assumptions of unlimited resources and conditions unchanging with time, the actual relationship between deGFP and MGapt is more complicated, a result of resource limits and changing environmental conditions. In Figure S11 we show deGFP(t^*) versus $\int^{t*}$MGapt, for $t^* = 1, 2, \ldots, 14$ hrs and for a range of Pr-deGFP-MGapt concentrations. As was also seen in Figure 1B, there are two operational regimes separated by a concentration threshold. Below 5nM plasmid DNA—the previously-described 'linear' regime in which $[\text{deGFP}]_{end}$ scales linearly with the DNA template concentration—$\int^{t*}$MGapt is proportional to deGFP(t^*) until protein synthesis stops at t^* ∼330 minutes (even though transcriptional activity continues). It is only during this period of time that transcriptional activity is a good predictor of what happens at the level of translation. Above the threshold concentration, in the 'saturation' regime where $[\text{deGFP}]_{end}$ is sublinear with respect to the amount of DNA template, protein production continues for longer and the $\int^{t*}$MGapt plateau is shorter than in the 'linear' regime. Precisely why protein production is sharply cut-off at low template concentrations and extended (albeit at a reduced rate) at high template concentrations, is unknown. But for circuit design and testing applications, these empirical results are worth noting: one can expect linear response at the translation level up to a fixed time only when operating in the 'linear' regime, and while protein production can continue for longer times when template concentration lies in the 'saturation' regime, the response is sublinear.

The effect of additional Pr-σ^{70} on $\int$MGapt and $[\text{deGFP}]_{end}$

The overall effect of additional Pr-σ^{70} is nonintuitive and dependent on both the Pr-σ^{70} and reporter concentrations. $[\text{deGFP}]_{end}$ versus $\int$MGapt for the baseline construct with various concentrations Pr-σ^{70} is shown in Figure S12. Compared with standard conditions, we see that low levels of Pr-σ^{70} (0.1–0.5 nM) lead to increased $\int$MGapt/decreased $[\text{deGFP}]_{end}$ with 10 nM reporter, decreased $\int$MGapt/increased $[\text{deGFP}]_{end}$ with 2 nM reporter, and an increase in $[\text{deGFP}]_{end}$ with no change in $\int$MGapt with 1 nM reporter. The system shows signs of being overburdened by 1 nM Pr-σ^{70} DNA, with relative decreases in both $\int$MGapt and $[\text{deGFP}]_{end}$ for all reporter concentrations. This would suggest that the substantial amount of additional DNA may be sequestering away resources required for reporter production, even if in this case the DNA codes for proteins that are ostensibly helpful.

Supplementary Figures

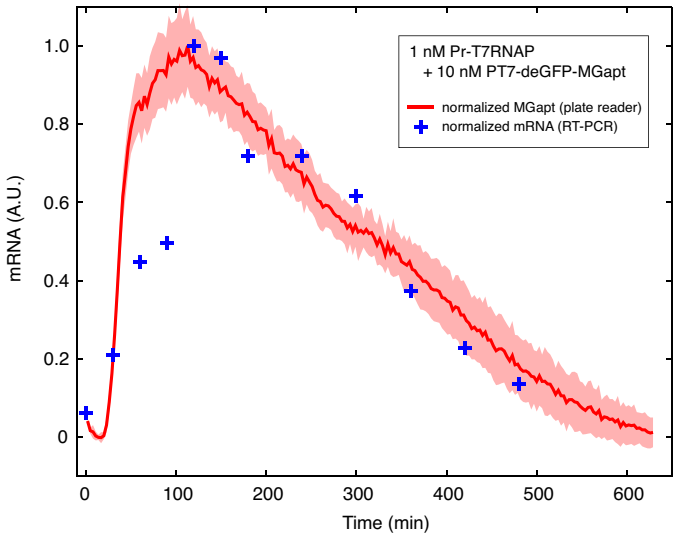

Figure S1: Comparison of normalized real-time PCR measurements and MGapt signal for T7 cascade circuit, with 1 nM Pr-T7 RNAP and 10 nM PT7-deGFP-MGapt.

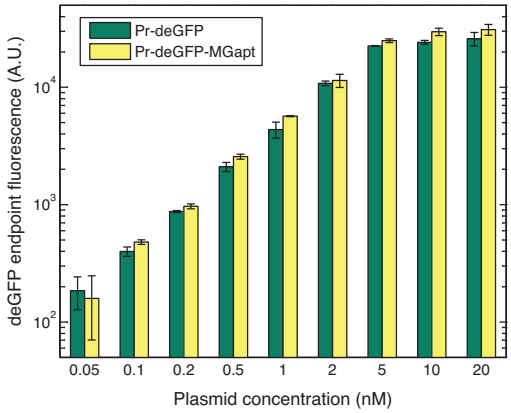

Figure S2: Comparison of total deGFP fluorescence produced by Pr-deGFP and Pr-deGFP-MGapt constructs. The incorporation of MGapt in the 3′ UTR downstream of deGFP leads to only a slight increase in the amount of protein produced relative to deGFP alone, a result we attribute to an increase in the stability of the fusion transcript conferred by the MGapt.

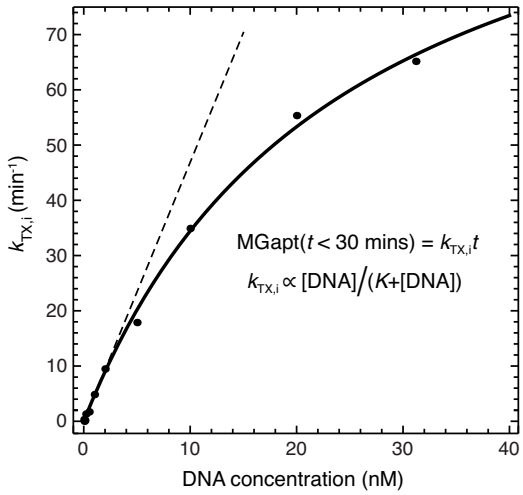

Figure S3: Rates of MGapt production in the first 30 minutes of expression follow a Michaelis-Menten form, saturating at high DNA concentrations. The Michaelis constant K is ∼24 nM.

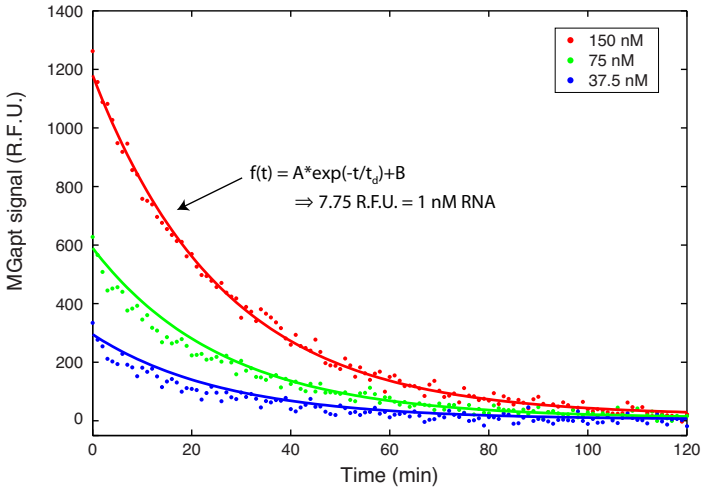

Figure S4: Decay curves for three different initial concentrations of purified deGFP-MGapt RNA.

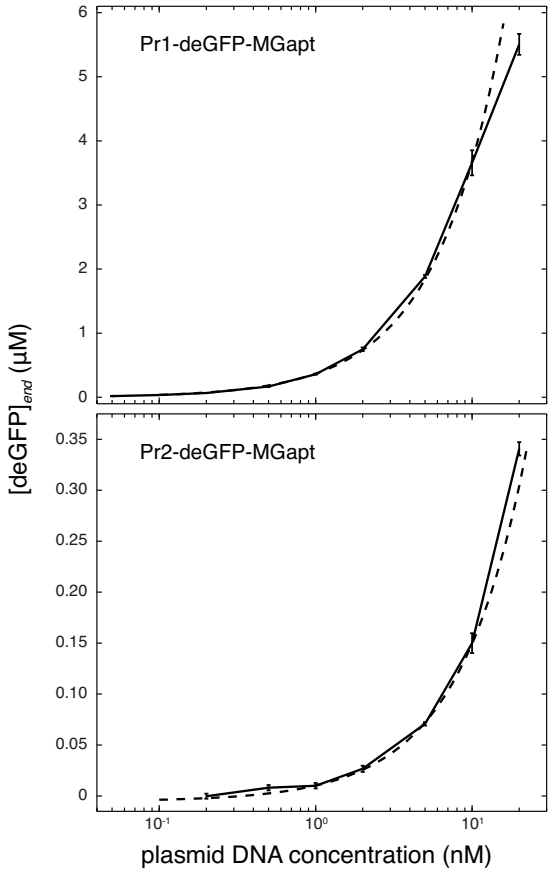

Figure S5: For deGFP-MGapt driven by weak promoters Pr1 and Pr2, the linear regime extends up to ∼10 nM and ∼20 nM, respectively. Dashed line shows a linear fit to the data.

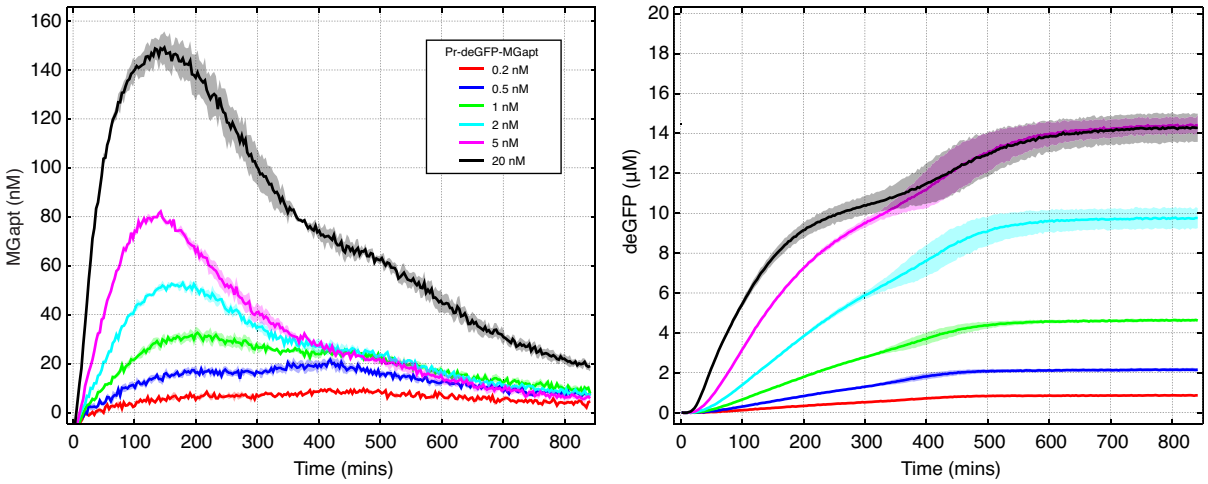

Figure S6: MGapt (left) and deGFP (right) expression kinetics when breadboard is supplemented with 1.25 mM of each of the four NTPs.

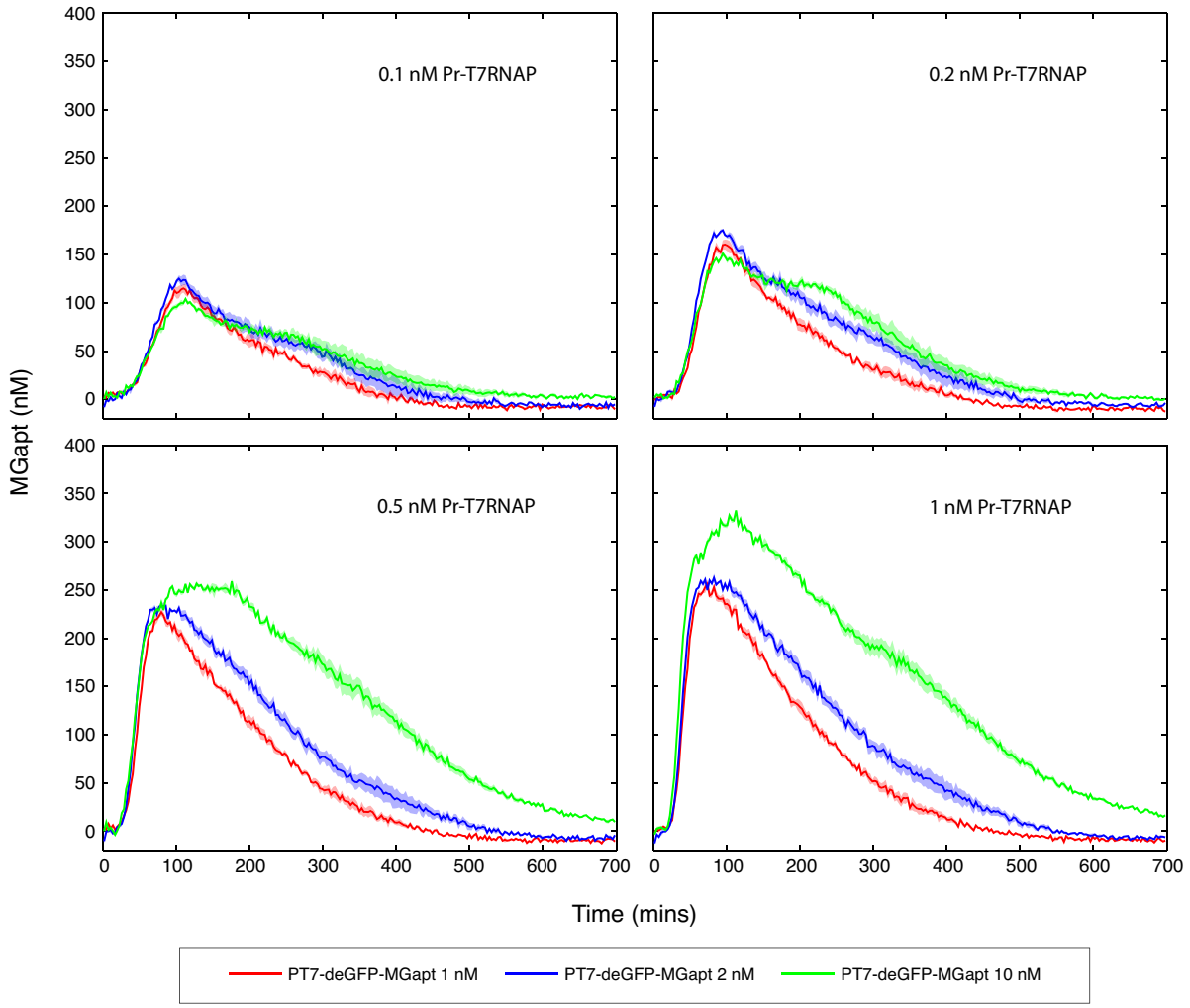

Figure S7: MGapt expression curves for T7 cascade tested with four different concentrations of first-stage T7 RNAP plasmid (0.1, 0.2, 0.5, and 1 nM Pr-T7 RNAP) and three different concentrations of the second-stage plasmid (1, 2, and 10 nM PT7-deGFP-MGapt).

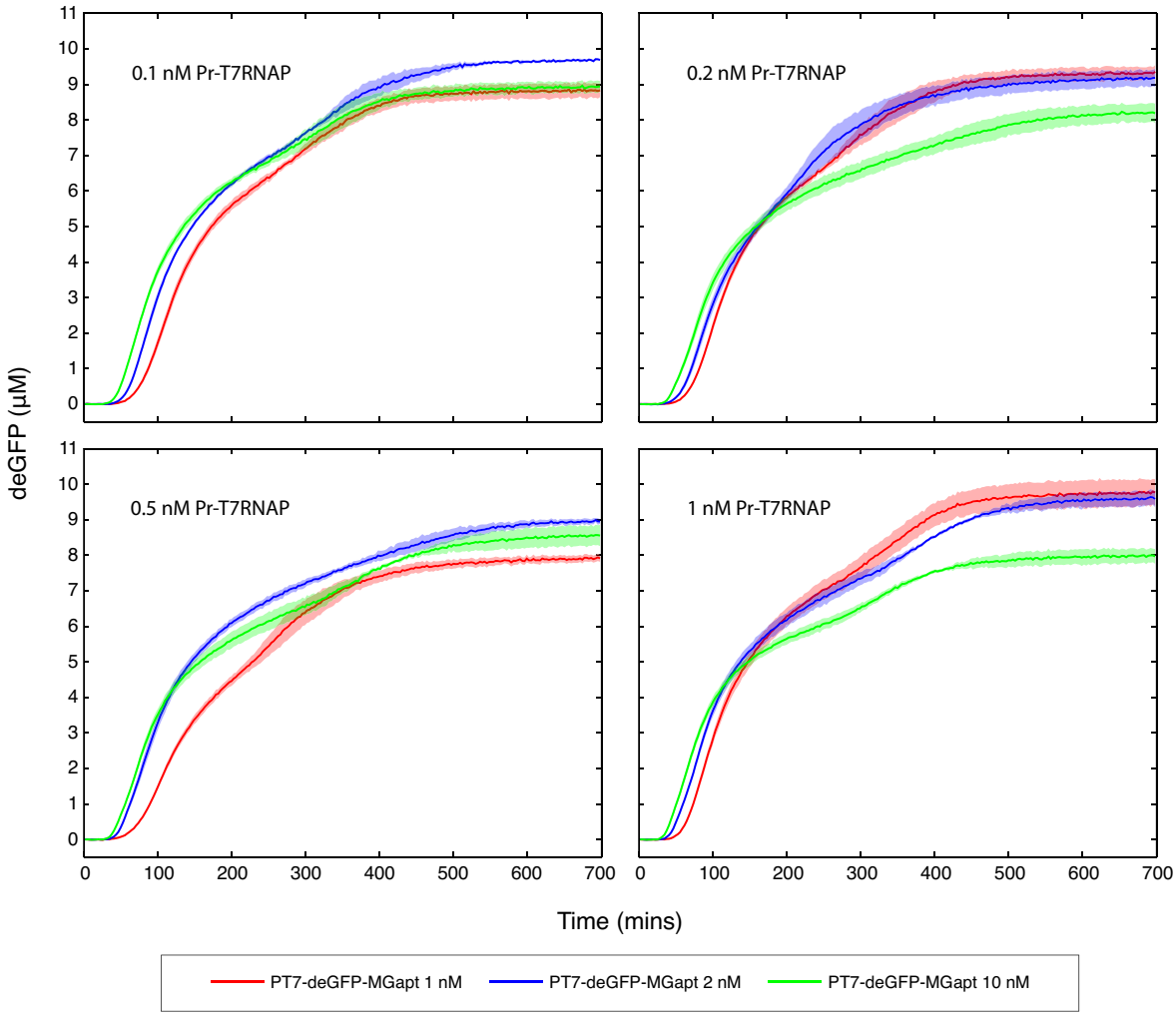

Figure S8: deGFP expression curves for T7 cascade tested with four different concentrations of the first-stage T7 RNAP plasmid (0.1, 0.2, 0.5, and 1 nM Pr-T7 RNAP) and three different concentrations of the second-stage plasmid (1, 2, and 10 nM PT7-deGFP-MGapt).

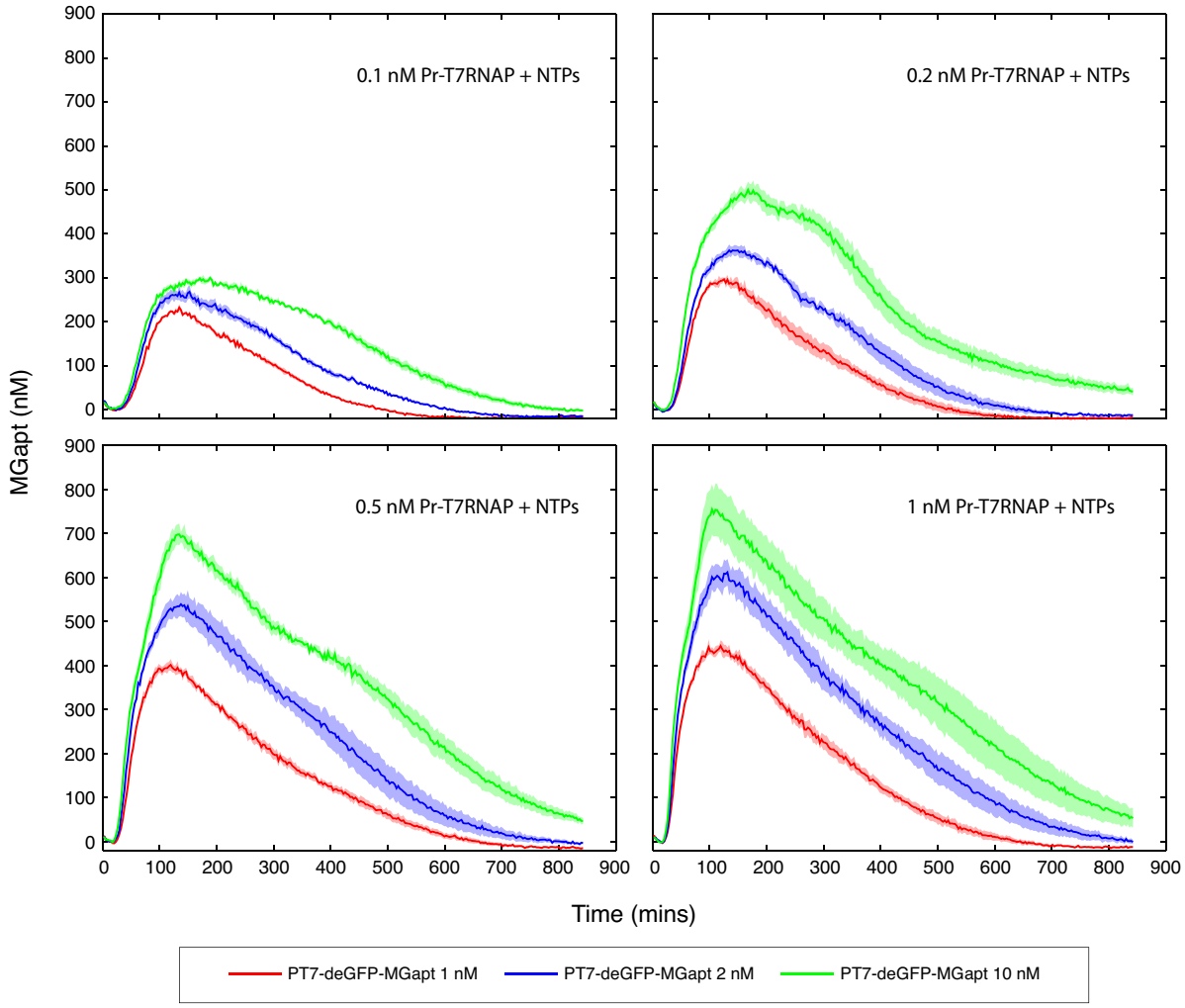

Figure S9: MGapt expression curves for T7 cascade tested with four different concentrations of first-stage T7 RNAP plasmid (0.1, 0.2, 0.5, and 1 nM Pr-T7 RNAP), three different concentrations of the second-stage plasmid (1, 2, and 10 nM PT7-deGFP-MGapt), and with the cell-free breadboard supplemented with 1.25 mM of each of the four NTPs.

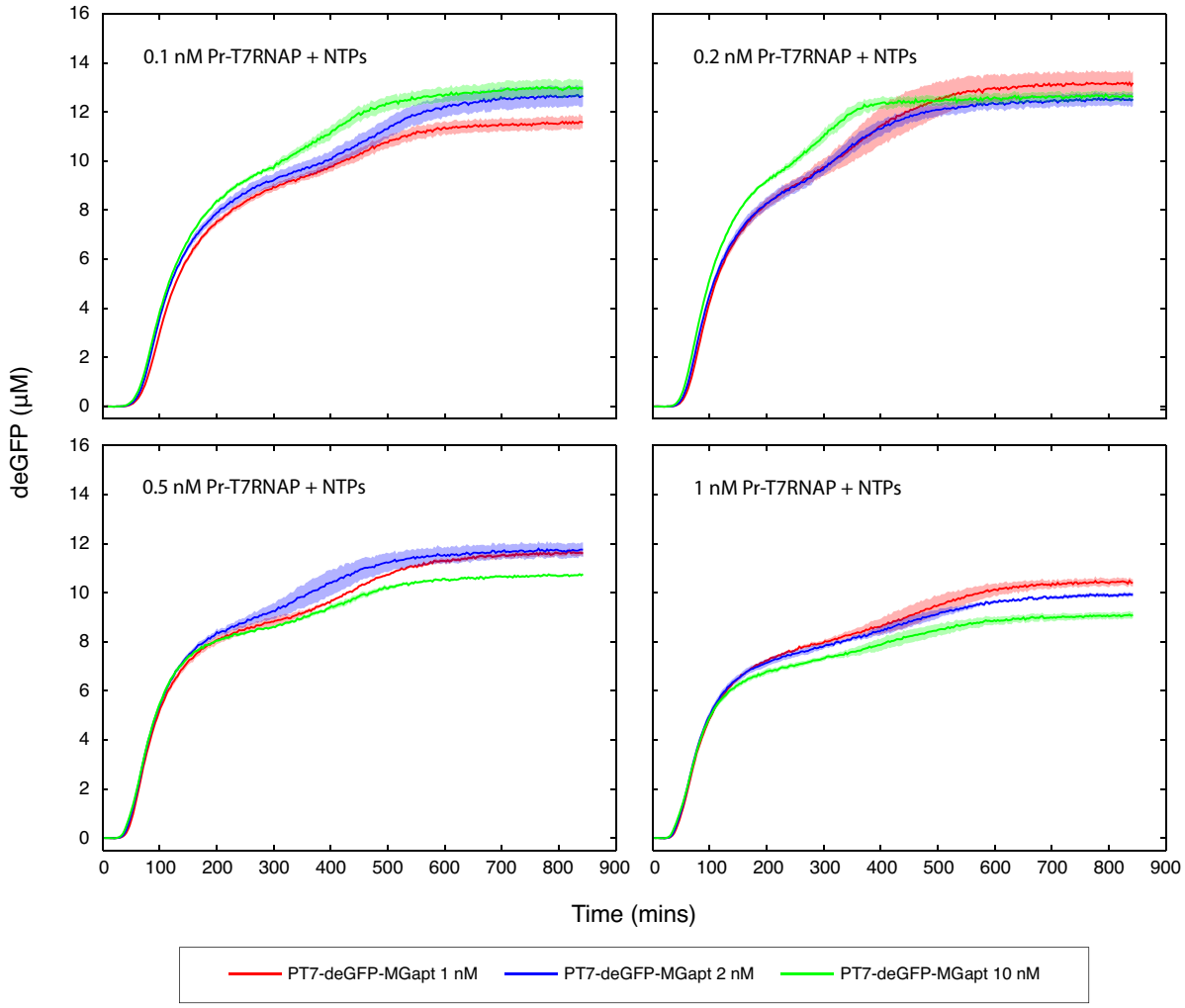

Figure S10: deGFP expression curves for T7 cascade tested with four different concentrations of the first-stage T7 RNAP plasmid (0.1, 0.2, 0.5, and 1 nM Pr-T7 RNAP), three different concentrations of the second-stage plasmid (1, 2, and 10 nM PT7-deGFP-MGapt), and with the cell-free breadboard supplemented with 1.25 mM of each of the four NTPs.

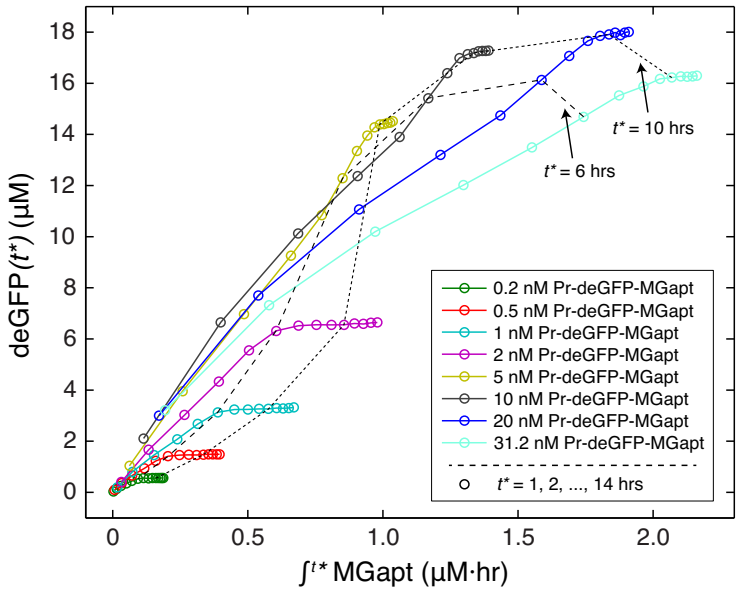

Figure S11: deGFP at various times t^* (deGFP(t^*)) versus MGapt level integrated from time $t = 0$ to $t = t^*$ ($\int^{t*}$MGapt) for a range of Pr-deGFP-MGapt concentrations, with $t^* = 1, 2, \ldots, 14$ hrs indicated with ○. Below the 'linear'–'saturation' regime transition concentration, $\int^{t*}$MGapt appears proportional to deGFP(t^*) until protein synthesis stops at t^* ∼330 minutes. Above the transition concentration, protein production stops later in the experiment and the $\int^{t*}$MGapt plateau is relatively short. Dashed lines showing $t^* = 6$ hrs and $t^* = 10$ hrs are shown for reference.

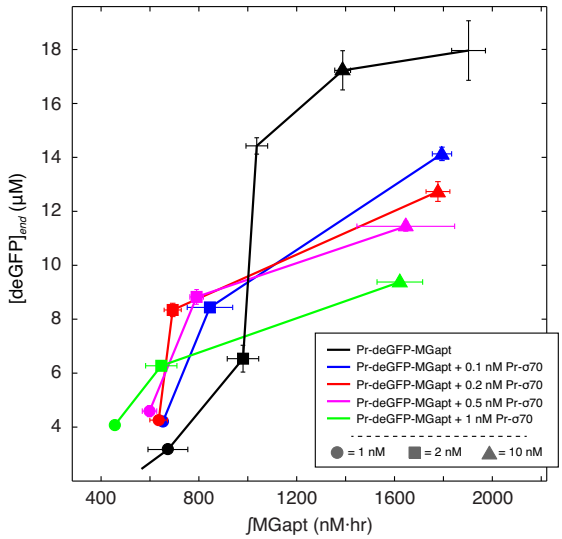

Figure S12: Endpoint deGFP versus integrated MGapt for Pr-deGFP-MGapt when the cell-free breadboard is supplemented with different concentrations of Pr-σ^{70} (● = 1 nM, ■ = 2 nM, ▲ = 10 nM). Relative to performance under standard conditions, low levels of Pr-σ^{70} (0.1–0.5 nM) lead to increased $\int$MGapt/ decreased $[\text{deGFP}]_{end}$ with 10 nM reporter, decreased $\int$MGapt/increased $[\text{deGFP}]_{end}$with 2 nM reporter, and an increase in $[\text{deGFP}]_{end}$ with no change in $\int$MGapt with 1 nM reporter. The system shows signs of being overburdened by 1 nM Pr-σ^{70} DNA, with relative decreases in both $\int$MGapt and $[\text{deGFP}]_{end}$ for all reporter concentrations.

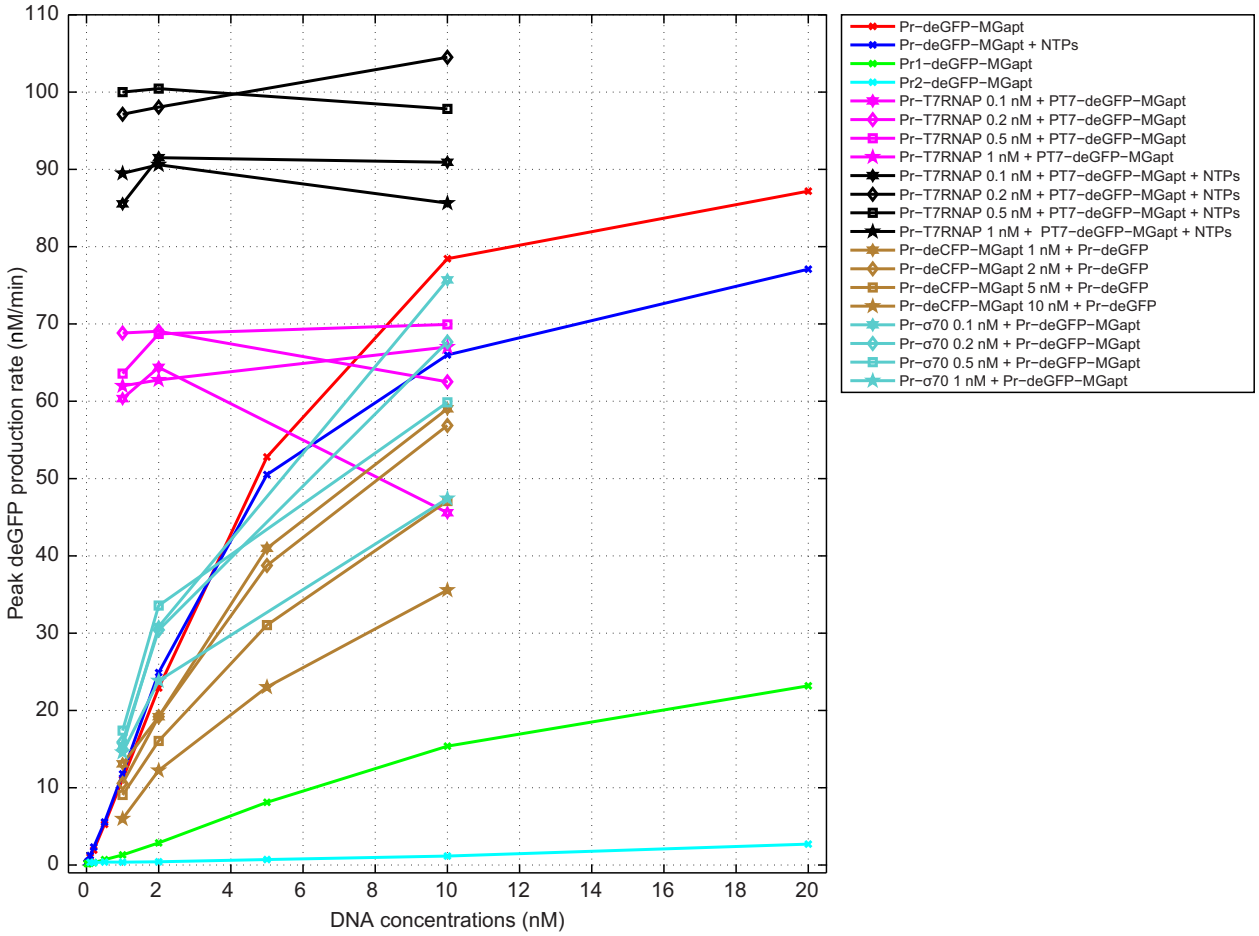

Figure S13: Maximum deGFP production rate as a function of reporter concentration under different conditions.

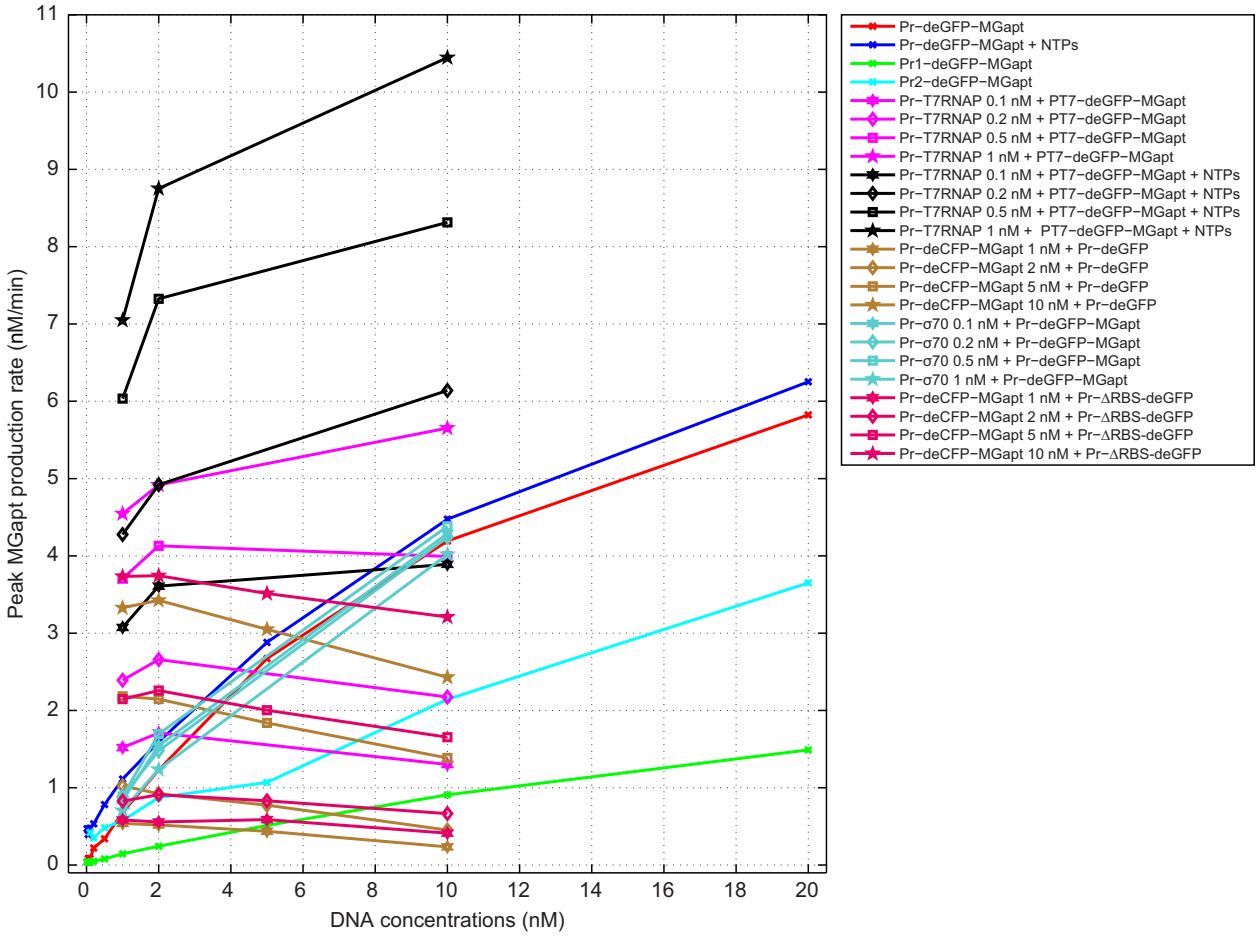

Figure S14: Maximum MGapt production rate as a function of reporter concentration under different conditions.

Supplementary tables

Table S1: Genotypes of the plasmids used in this study.

Plasmid name	ORFs	Backbone/resistance
pBEST-Pr-GFP	P_R:deGFP	ColE1/Amp^R
pBEST-Pr-ΔRBS-GFP	P_R:ΔRBS-deGFP	ColE1/Amp^R
pBEST-Pr-GFP-MG	P_R:deGFP-MGapt	ColE1/Amp^R
pBEST-Pr1-GFP-MG	P_{R1}:deGFP-MGapt	ColE1/Amp^R
pBEST-Pr2-GFP-MG	P_{R2}:deGFP-MGapt	ColE1/Amp^R
pBEST-Pr-CFP-MG	P_R:deCFP-MGapt	ColE1/Amp^R
pBEST-Pr-σ_{70}	P_R:σ_{70}	ColE1/Amp^R
pBEST-Pr-T7RNAP	P_R:T7 RNAP	ColE1/Amp^R
pBEST-Pr1-T7RNAP	P_{R1}:T7 RNAP	ColE1/Amp^R
pBEST-Pr2-T7RNAP	P_{R2}:T7 RNAP	ColE1/Amp^R
pIVEX-pT7-GFP-MG	P_{T7}:deGFP-MGapt	ColE1/Amp^R